

Research Paper

Optimal Load Distribution Based on Decision Theory with Information Gap in the Presence of Wind Farms Connected to the Power System

Kourosh Alijanzadeh and Ali Ghasemi-Marzbali * 

Department of Electrical and Biomedical Engineering, Mazandaran University of Science and Technology, Babol, Iran.

Abstract— Optimal load distribution in power systems is crucial for minimizing overall costs while adhering to technical constraints. This process becomes increasingly complex with the integration of wind energy due to the inherent uncertainty in wind turbine production caused by variable wind conditions. This paper presents a novel approach to address these uncertainties within the context of the optimal power flow (OPF) problem by employing Information Gap Decision Theory (IGDT). Unlike traditional scenario-based methods, IGDT provides a computationally efficient and reliable framework for decision-making under uncertainty without extensive probabilistic data. The methodology uses the Weibull probability density function to model wind speed, allowing for realistic estimation of wind farm output power. The Evolutionary Particle Swarm Optimization (EPSO) algorithm, an advanced version of PSO, is utilized to solve the optimization problem, reducing the risk of convergence to local optima. Results are computed under two strategies: risk-averse and risk-taking, represented by immunity functions. These strategies highlight the impact of user demand on adjusting calculation parameters. Comparative analysis with scenario-based probabilistic optimization shows that the IGDT approach enhances system load cost evaluation by 0.12%. This study provides a robust framework for optimal power allocation under uncertainty, ensuring resilient and secure power generation.

Keywords—Optimal load distribution, decision theory with information gap, uncertainty, wind farm.

NOMENCLATURE

$\bar{\gamma}$ Mean of uncertain parameter
 δ (rad) Voltage angle
 Γ Uncertain parameter vector
 $\hat{\alpha}$ Maximum uncertainty parameter value
 $\hat{\beta}$ Minimum value of the uncertainty parameter
 ρ (kg/m³) Air density
 φ (rad) Admission angle
 $\varphi(t)$ An arbitrary known function
 ξ Radius of uncertainty
 C_k (\$) Maximum power supply cost
 C_w (\$) Maximum cost of power supply for profitability
 G_{best}^k The best value among the total particles in iteration k
 I_i (A) Injectable reactive power
 N_G Number of power-plant buses
 N_L Number of bus consumed
 $P_D(W)$ Consumption load of the whole network
 $P_{Gi}(VAR)$ Reactive power generated by the thermal unit
 $P_{Gi}(W)$ Active power generated by the heating unit

$P_{ij}(W)$ Power passing between buses i and j
 $P_i(W)$ Injectable active power
 $P_{Loss}(W)$ Network losses
 $P_{wind}(W)$ Wind turbine production capacity
 $P_{best}^k_j$ The best memory value of a j particle in iteration k
 Q_C Compensator production power
 $Q_i(VAR)$ Injectable reactive power
 TC_b The main value of the objective function
 TP^{max} Maximum tap trans
 TP^{min} Minimum trans beat
 $V_i(V)$ Injection flow
 V_{cut-in} (m/s) Start speed of wind turbine power generation
 $V_{cut-out}$ (m/s) Completion speed of wind turbine power generation
 V_{rated} (m/s) Nominal speed of wind turbine power generation
 V_{wind} (m/s) Direct wind speed
 x_j^k The consequence of the j particle in the iteration k
 α_i (\$) Fixed cost of the power-plant
 β_i (\$/W) Power-plant's power cost factor
 γ_i (\$/W²) Quadratic coefficient of power-plant's power cost
 Λ_c (\$) Critical value
 Λ_o (\$) The amount of opportunity
 \bar{u} Mean value of uncertain parameter
 $\hat{u}(t)$ Nominal value of uncertain parameter
 $\tilde{p}(u)$ Uncertainty function of probability distribution
 \tilde{u} Nominal value of uncertain parameter
 σ_γ Variance of uncertain parameter
 σ_j' Outcome range generated around parent j
 σ_u Variance of uncertain parameter
 ς_c The degree of tolerance allowed in increasing the cost
 ς_o The degree of greed in further improving of objective function

Received: 17 Apr. 2024

Revised: 10 Jun. 2024

Accepted: 24 Jun. 2024

*Corresponding author:

E-mail: ali.ghasemi@ustmb.ac.ir (A. Ghasemi-Marzbali)

DOI: 10.22098/joape.2024.14914.2140

This work is licensed under a [Creative Commons Attribution-NonCommercial 4.0 International License](https://creativecommons.org/licenses/by-nc/4.0/).

Copyright © 2025 University of Mohaghegh Ardabili.

c_1	Velocity coefficient of the best total value
c_2	velocity coefficient for best memory of each particle
f_b (\$)	The main value of the cost function
K_δ (rad/A)	Voltage angle coefficient of maximum transmission power
K_v (Ω)	Voltage magnitude coefficient of maximum transmission power
N_j (0, 1)	Gaussian random variable with mean zero and standard deviation 1
P_{Gi}^{\max} (W)	Minimum active power output of the heating unit
P_{Gi}^{\min} (W)	Maximum reactive power produced by the heating unit
P_{ij}^{\max} (W)	Maximum throughput between buses i and j
P_{WF} (W)	Wind farm active power
P_{wg}^f (W)	Average wind farm power
P_{wg}^{avl} (W)	Power available to wind farm
Q_{Gi}^{\max} (VAR)	Minimum reactive power produced by the thermal unit
V_j^k	The velocity of the particle j in the iteration k
x_j^k	The location of the j particle in the iteration k
y_{ij} (1/ Ω)	Bass voltage
y_i (1/ Ω)	Maximum active power output of the heating unit
A	Constant value of Q-P wind farm curve
A (m^2)	Area swept by the blades
B	Q-P curve shape coefficient of wind farm
C	The scale parameter in the weibull probability density function
C (\$)	Power supply cost
D	Consumption load index
FT	Compatibility function
G	Production power index
I	Bass index
K	The shape parameter in the weibull probability density function
maxIT	Maximum number of iteration
nPop	Population in PSO
Q	Decision variable vector
TC	The objective function
TP	Tap trans
U	Uncertain parameter vector
u(t)	Uncertain parameter or function
V	The positive matrix of a symmetric real entity
W	Inertia coefficient
Wdamp	Speed drop coefficient
X	A set of decision variables
X	State variables vector
	Uncertainty modeling parameter

1. INTRODUCTION

1.1. Background and aims

Today, wind energy is widely regarded as one of the most prominent sources of pollution-free renewable energy. Wind energy exhibits both time-varying and unpredictable characteristics. When the penetration of renewable energy sources in the power system is low, variations in wind conditions are somewhat tolerable. However, as this penetration reaches higher levels, the consequential impact of these changes becomes more pronounced, necessitating the incorporation of additional generators to balance load distribution [1]. A particular challenge arises when a wind turbine is connected to a weak system or distribution feeder. In such instances, the issue of cycling and the inherent short-term changes associated with wind production can be addressed through the use of energy accumulators. The application of wind power generation technology, driven by economic and environmental concerns, has garnered significant attention worldwide. The primary objective of the system operator is to manage the network in a manner that minimizes the total cost of power generation under given user conditions, while also meeting technical and operational

constraints. This optimization problem is commonly referred to as Optimal Power Flow (OPF) [2]. Effectively modeling the uncertainty linked to wind power generation is a critical aspect of the OPF formulation. Therefore, accurate modeling of wind energy production within the OPF framework is essential. As mentioned, the utilization of wind energy brings numerous benefits, such as reducing the cost of energy supply and minimizing environmental pollution. However, the inherent uncertainty in wind energy generation has a notable impact on the performance of systems utilizing this energy to meet load demand [3].

1.2. Literature review

In [4], a multiobjective reactive power planning, taking into account the uncertainties in load demand and wind power generation is proposed. The primary focus is to examine the impact of these multiple uncertainties on Reactive Power Planning (RPP) while considering various objectives. To achieve this, IGDT is employed to manage the uncertainties associated with load demand and wind power production. In [5], an efficient bi-level energy management strategy (EMS) to minimize the operation cost of a grid-connected microgrid, accounting for system constraints and uncertainties in renewable energy sources and load demand is presented. The first level involves optimal day-ahead scheduling in two stages: determining the optimal operating points of sources and managing controllable loads. The second level focuses on real-time rescheduling and updating of source set-points based on actual solar irradiance, wind speed, load, and grid tariff.

In [6], a probabilistic multi-objective economic-environmental utilization planning model for energy planning and storage in an intelligent distribution system with high wind penetration is introduced. In [7], a technique for optimizing power system operation amidst rising energy demands is discussed. It integrates demand response programs (DRPs), distributed generation (DG) installation, and DC dynamic load flow analysis. The model aims to reduce congestion, improve available transfer capability (ATC) rates, and incentivize customers to adjust consumption patterns through price-based DRPs.

In [8], a risk-based stochastic optimal energy management model for a microgrid incorporating renewables, energy storage, and load control through time-of-use demand response (DR) programs is developed. The microgrid features a PV system, wind system, micro-turbine, fuel cell, electric vehicle (EV), and energy storage. To manage load uncertainties and devise operating strategies for the microgrid's controllable energy resources, IGDT is utilized. In [9], the study focuses on designing and presenting a hierarchical automatic voltage control system and wind farm operation area to address significant voltage fluctuations and wind generator errors, which pose considerable challenges. For each wind farm, an automatic Wind Farm Voltage Controller (WFVC) is implemented to optimize the voltage and reactive power distribution within the wind farm. Subsequently, the necessities and challenges of the Automatic Voltage Control (AVC) method to support high integration of wind power are also discussed. In [10], a two-layer framework for optimal islanding operation of a multi-energy microgrid (MG) integrated with prosumer hybrid renewable systems (HRSSs) is proposed. Each HRS, equipped with technologies such as solar panels, batteries, hydrogen storage, and electrolyzers, can exchange power with the MG. In the first layer, the robust self-scheduling problem for each HRS is solved independently to determine the optimal electricity transactions with the upstream MG, accounting for electricity price uncertainties. In [11] was tackled challenges caused by the unpredictable and probabilistic nature of wind speed and solar irradiance, which lead to variable power production in renewable sources. These variations create power imbalances in grids due to the difficulty of accurate estimation. The study presents an enhanced data-driven uncertainty set, employing a neural network trained with extensive historical data from a multi-microgrid system.

In [12], a stochastic optimization model for local integrated hydrogen-power energy systems is suggested. The model aims to minimize day-ahead operation costs by utilizing dispatchable resources, renewable energy sources, battery energy storage systems, demand response programs, and energy trading with the upstream network. Additionally, the integrated system can trade electricity with the upstream network for increased benefits. In [13], a risk-based robust energy scheduling model for microgrids to manage the uncertainty of renewable energy sources (RESs) is addressed. The model introduces a novel adjustable convex hull-based uncertainty set (ACHUS), which quantifies RES uncertainty as a subset of the maximum uncertainty set. The operational risk of an ACHUS is assessed using a historical data-based method. This method defines operational risk as the expected penalty cost of all historical data, ensuring the microgrid's operational safety within the ACHUS.

In [14], a multi-objective function is proposed to address the nonlinear problem of determining the optimal location and size of the wind farm. The target function is formulated to minimize the number of wind farms and power losses while maximizing the voltage stability margin. The proposed method accounts for power system limitations, including passing power limits of the lines and bus voltages. Additionally, the method can adaptively apply reactive power limitations to wind farms. In [15], a multi-objective algorithm is introduced to assess the impact of location and optimal wind size in enhancing the distribution system's performance with respect to loss reduction under different load models in distribution systems. The proposed algorithm focuses on wind cost reduction and improving the voltage profile as its target functions. The algorithm's performance is investigated on a reference system.

In [16], a decentralized coordinated dispatch model aimed at multiple stakeholders within the system is suggested. This model considers energy interactions among Micro energy grids (MEGs) and addresses the inherent uncertainty linked with renewable energy sources. Specifically, a stochastic optimization approach was employed to characterize the uncertainty of renewable energy output by generating stochastic scenarios. In [17], a novel model for a local energy market structure comprising an aggregator, prosumers, electricity, gas, and heat utility grids, and consumers is introduced. The interactions among these entities are managed using an auction model with suggested bidding strategies, allowing each participant to maximize their individual objective function. In [18], the authors describe the initial quantification method for solving the optimal load distribution with a genetic algorithm. The results show that the proposed initial quantification method in the GA-OPF implementation improves the values of the target function.

In [19], a thorough analysis of a hybrid wind and PV system, emphasizing the attainment of consistent DC bus-bar voltage through integration with a microcontroller system via a buck-boost converter is offered. Moreover, the hybrid system's output voltage is customized to accommodate required battery connections. However, due to environmental variables such as fluctuations in solar irradiation and wind velocity impacting the power output of PV and wind, seamless integration of these sources becomes crucial. In [20], the authors formulate transient constant constraints on the optimal load distribution problem. Studies describe a PSO approach for solving the problem of optimal load distribution with security constraints and transient constant constraints in the system. Case studies show that PSO is a viable alternative to the challenging OPF problem. In [21], a three-stage robust optimization model for multi-energy microgrids (MEMs) to enhance flexibility and robustness is proposed. Firstly, source-load uncertainties are addressed with a data-driven approach, including electric vehicle uncertainties using clustering. Secondly, a three-stage min-max robust optimization model is developed, considering multiple uncertainties and interaction with EV users using game theory. Finally, the model is solved using the column and constraint generation algorithm, and numerical simulations are conducted

based on a real energy park model. In [22], a multi-objective harmony search algorithm for the optimal load distribution problem is investigated. The computational results demonstrate that the proposed method not only ensures the operation constraints but also calculates lower fuel costs compared to other methods. In [23], the EPSO evolutionary optimization algorithm is employed for optimal load distribution in an IEEE modified 30-bus network, considering both wind and thermal power plants. The method for modeling the output power uncertainty of wind farms is based on the power curve in terms of the third degree of velocity, utilizing the Weibull probability density function from information obtained through HOMER energy optimization software. Additionally, the algorithm addresses the OPF problem while considering the rotating reservation constraint. The results indicate the effectiveness of the method used, although it lacks a specific decision-making strategy like IGDT, limiting its versatility across different situations with varying degrees of satisfaction. In [24], a method to solve the problem of optimal load distribution involving offshore wind farms connected to the HVDC network is presented. Various factors are considered in the proposed method, including the connection limitations of the voltage source converter with HVDC voltage (VSC-HVDC) and the linearly commutated converter with HVDC voltage (LCC-HVDC), the capacity curve of the two-way power induction generator (DFIGs), and wind energy generation uncertainties. Information gap decision theory (IGDT) is utilized to address uncertainties related to wind energy fluctuations. Table 1 presents a comparison of each study:

1.3. Previous researches gaps and suggested contributions

The literature on the impact of uncertainty in decision-making on the optimal power flow (OPF) of wind-thermal power systems reveals several significant gaps. Few studies have thoroughly examined how wind production influences OPF utilization, bus voltage, and transmission line losses, despite the notable effect of wind generation system locations on these factors. Additionally, there is a lack of comprehensive research on the economic utilization of power systems in relation to wind production, particularly concerning its impact on bus voltage and transmission losses. Most existing studies rely on scenario-based methods to address wind farm output uncertainty, which may not fully capture the complexities involved. The use of IGDT to manage uncertainties is relatively new and underexplored, and while IGDT can aid decision-makers in prioritizing and evaluating risks with minimal information, its application in this context remains limited. Furthermore, previous works lack a thorough evaluation of proposed solutions for optimal load distribution in the presence of wind power plants, resulting in an unclear understanding of their efficiency [25]. Addressing these shortcomings requires integrating economic considerations, system performance metrics, and advanced uncertainty management techniques such as IGDT in future studies.

To address the identified gaps and shortcomings in the literature, this paper investigates the problem of optimal power load distribution under the uncertainty of wind farm power generation and its impact on network parameters. To model wind farm production uncertainty, the Weibull probability density function, which accurately represents wind speed distribution, is utilized. By determining the scale and shape parameters of the Weibull function based on regional conditions, the output power of each turbine is calculated from the cubic relationship between power and wind speed. A piecewise probability function is then derived for the turbine output power, and the output power probability function for the entire wind farm is established by correlating the turbines. This analysis employs Information Gap Decision Theory (IGDT) to handle uncertainty. Using a robust, risk-averse model, the maximum uncertainty in extractable wind energy is identified in exchange for a slight increase in operating costs. Conversely, an opportunistic, risk-taking model determines the

Table 1. A comparison of previous papers.

Ref.	Advantages	Disadvantages
[4]	- Considers various objectives in Reactive Power Planning (RPP). - Utilizes Information Gap Decision Theory (IGDT) to manage uncertainties.	- Limited discussion on the practical implementation of proposed strategies. - May require extensive computational resources for optimization.
[5]	- Minimizes operation cost and improves system efficiency. - Implements optimal day-ahead scheduling and real-time rescheduling. - Accounts for uncertainties in renewable energy sources and load demand.	- Complexity in real-time implementation of rescheduling strategies. - Potential challenges in integrating real-time data for decision-making.
[6]	- Addresses economic and environmental aspects of energy planning. - Proposes a probabilistic multi-objective optimization approach.	- Limited validation on real-world data and scenarios. - Complexity in modeling economic and environmental factors.
[7]	- Reduces congestion and improves available transfer capability rates. - Incentivizes demand response participation. - Considers various factors influencing power system operation.	- Scalability challenges in large-scale implementation. - Limited discussion on regulatory aspects and market dynamics.
[8]	- Minimizes operation cost and enhances system efficiency. - Manages uncertainties in renewable energy sources and load demand. - Utilizes Information Gap Decision Theory (IGDT).	- Limited exploration of model's performance under diverse operating conditions. - Potential complexity in implementing IGDT-based strategies.
[9]	- Optimizes voltage and reactive power distribution within wind farms. - Addresses challenges of wind power integration. - Discusses Automatic Voltage Control (AVC) methods.	- Limited scalability of discussed solutions to large wind farms. - Potential challenges in real-world implementation of AVC methods.
[10]	- Enhances microgrid resilience and energy autonomy. - Implements robust self-scheduling for optimal electricity transactions. - Addresses uncertainties in electricity prices.	- Potential challenges in coordinating transactions among hybrid renewable systems (HRSs). - Complexity in real-time decision-making based on price uncertainties.
[11]	- Improves accuracy of renewable energy forecasting. - Enhances stability in multi-microgrid systems. - Employs enhanced data-driven uncertainty set for modeling uncertainties.	- Computational complexity in training neural networks with historical data. - Limited discussion on real-time implementation challenges.
[12]	- Minimizes operation costs and optimizes energy trading. - Utilizes stochastic optimization approach for modeling uncertainties.	- Limited exploration of model's adaptability to dynamic market conditions. - Complexity in integrating multiple energy trading strategies.
[13]	- Ensures microgrid's operational safety under uncertainties. - Introduces novel adjustable convex hull-based uncertainty set (ACHUS). - Addresses uncertainties in renewable energy sources (RESs).	- Potential computational complexity in evaluating ACHUS. - Limited validation on real-world microgrid systems.
[14]	- Enhances grid efficiency and stability. - Considers various power system limitations in wind farm optimization. - Adapts reactive power limitations based on operational conditions.	- Complexity in formulating and solving multi-objective optimization problems. - Potential challenges in real-world implementation of proposed solutions.
[15]	- Improves integration of wind energy into distribution systems. - Reduces wind cost and improves voltage profile. - Utilizes multi-objective algorithm for assessing wind farm impact.	- Limited exploration of model's robustness under diverse load and weather conditions. - Complexity in calibrating algorithms for specific distribution system configurations.
[16]	- Enhances coordination and stability of micro energy grids (MEGs). - Considers uncertainties in renewable energy output. - Employs stochastic optimization approach for characterizing uncertainties.	- Scalability challenges in large-scale implementation. - Computational complexity in generating stochastic scenarios.
[17]	- Promotes efficient and fair energy market operations. - Maximizes individual objective functions of market participants. - Utilizes auction model with suggested bidding strategies.	- Limited discussion on adaptability of auction model to diverse market conditions. - Potential challenges in implementing suggested bidding strategies.
[18]	- Improves values of target function in optimal load distribution. - Utilizes initial quantification method for enhancing optimization. - Implements genetic algorithm for solving load distribution problem.	- Complexity in scaling up solutions to large-scale power systems. - Potential challenges in real-world implementation of genetic algorithm-based solutions.
[19]	- Addresses challenges in integrating hybrid wind and PV systems. - Emphasizes consistent DC bus-bar voltage and battery integration. - Discusses environmental impact on renewable energy systems.	- Limited discussion on real-world performance of proposed integration strategies. - Challenges in adapting solutions to diverse environmental conditions.
[20]	- Provides viable alternative for solving challenging optimal load distribution problem. - Utilizes PSO approach for addressing security constraints and transient constant constraints. - Demonstrates applicability of PSO in optimal load distribution.	- Potential challenges in optimizing PSO parameters for specific system configurations. - Limited exploration of PSO's performance under diverse operating conditions.
[21]	- Enhances flexibility and robustness of multi-energy microgrids (MEMs). - Addresses uncertainties using data-driven approach and game theory. - Utilizes column and constraint generation algorithm for solving robust optimization model.	- Complexity in integrating multiple stages of robust optimization. - Scalability challenges in large-scale MEM implementation.
[22]	- Ensures operation constraints and lower fuel costs in load distribution. - Investigates multi-objective harmony search algorithm for optimization. - Demonstrates improved performance compared to other methods.	- Limited exploration of model's performance under diverse operating conditions. - Challenges in adapting harmony search algorithm to large-scale power systems.
[23]	- Addresses uncertainties in wind power output and HVDC network integration. - Utilizes PSO evolutionary optimization algorithm for load distribution. - Considers rotating reservation constraint in optimizing load distribution.	- Lack of specific decision-making strategy like IGDT, limiting versatility across different situations. - Potential challenges in scaling up PSO solutions.
[24]	- Addresses uncertainties related to wind energy fluctuations. - Considers various factors including HVDC network limitations and wind energy generation uncertainties. - Utilizes Information Gap Decision Theory (IGDT) for addressing uncertainties.	- Limited exploration of real-world application and validation. - Potential challenges in scaling up IGDT-based solutions.

minimum uncertainty in exchange for reduced operating costs. The proposed method outputs the optimal generating capacity of network power plant units, considering renewable resource uncertainties, ensuring a resilient and stable power generation plan. Here are the key contributions summarized:

- 1) Recognizing the uncertainty in wind turbine production due to variable wind conditions, the paper proposes a method that integrates IGDT into the OPF problem. This approach helps in making decisions under uncertainty without relying heavily on probabilistic data.
- 2) Unlike traditional scenario-based methods, IGDT offers a computationally efficient and reliable framework for decision-making. It doesn't require extensive probabilistic data, making it suitable for addressing uncertainties efficiently.
- 3) The methodology employs the Weibull probability density function to model wind speed, allowing for realistic estimation of wind farm output power. This enhances the accuracy of predictions regarding wind energy generation.
- 4) The paper utilizes the EPSO algorithm, an advanced version of PSO, to solve the optimization problem. This algorithm reduces the risk of convergence to local optima, ensuring more robust results.
- 5) The study explores two strategies: risk-averse and risk-taking, represented by immunity functions. These strategies

consider the impact of user demand on adjusting calculation parameters, offering insights into how different approaches affect decision-making under uncertainty.

1.4. Paper layout

The rest of this paper is organized as follows: Section 2 explains the main components of IGDT decision models. Section 3 covers optimal load distribution modeling, describing techniques and case studies. Section 4 introduces the modified PSO algorithm and its application in optimization. Section 5 presents and analyzes simulation results, evaluating performance metrics. Finally, Section 6 summarizes the key findings and discusses future research directions.

2. THE MAIN COMPONENTS OF IGDT DECISION MODELS

The main components of a decision-making problem using the IGDT method are divided into three parts as follows:

2.1. System model

The system model articulates the input-output structure of the decision-making process. In other words, the system model

examines how the system responds to the decisions made by the decision-maker and the uncertain parameter according to various criteria. The system model can encompass engineering design, reliability parameters, project management, and economic issues. In the case study of this thesis, the system model represents the function of the supply cost or purchase of energy, which is a function of the energy supply cost from different resources. By assuming q as decision variables, u as the uncertain parameter, \tilde{u} as the nominal value or the predicted uncertainty parameter, and α as the uncertainty modeling parameter, the system model will be a function of q, u as follows:

$$\begin{aligned} C &= (q, u) = C(q, \tilde{u}, \alpha) \\ u &= U(\tilde{u}, \alpha) \end{aligned} \quad (1)$$

Where $C = (q, u)$ represents the system model - the cost of power supply.

2.2. Performance requirements

These requirements articulate the essential expectations or specifications of the system or the matter at hand and are formulated as a cost function or other functions. These requirements are assessed based on the "resistance" and "opportunity" functions, and thus the optimization definition of these functions will be grounded in the system requirements. It is essential to note that, according to the system model and expectations, one of these functions has the property of risk-seeking, while the other, conversely, has the property of risk-taking [26]. For the specific issue addressed in the thesis, the resistance function, denoted by $\hat{\alpha}(q, C_k)$, represents the maximum value of the parameter expressing uncertainty for which the highest cost of energy supply does not exceed a certain value. In other words, the goal is to find a value of the parameter α that signifies decision-making resistance to the high cost of energy supply, and, consequently, a larger amount of it is considered. Therefore, the intended function can be mathematically defined as follows:

$$\hat{\alpha}(q, C_k) = \max_q \left\{ \alpha : \max_{u \in U(\alpha, \tilde{u})} C(q, u) \leq C_k \right\} \quad (2)$$

It is observed that the above definition expresses a maximization function, and based on it, both the value of the function and the values of the decision variables are obtained. Moreover, the opportunity function, denoted by $\beta(q, C_w)$, represents the lowest value of the uncertainty indicator parameter for which the lowest cost of power supply is less than a certain value. In other words, this function expresses the lowest value of α in which low energy supply costs are possible, and therefore its small value is desirable. Therefore, this function can be mathematically defined as follows:

$$\beta(q, C_w) = \min_q \left\{ \alpha : \min_{u \in U(\alpha, \tilde{u})} C(q, u) \leq C_w \right\} \quad (3)$$

It is evident that the minimization function aims to find the decision variables and the magnitude of the opportunity function. After performing the aforementioned optimizations, the value of the uncertain parameter can be calculated according to the definition of the uncertainty model.

2.3. Uncertainty model

The uncertainty model incorporates prior information about the uncertain parameter. In many cases, it is sufficient to consider a simple and general model, but in some cases, hybrid models can be employed. The intended uncertainty is typically expressed in terms of the predicted value of that parameter and the uncertainty parameter. It should be noted that uncertainty models are not limited to the mentioned models, and for more information, one can

Ref. to [27]. In this paper, the referred models of envelope-bound and models based on mean and variance in the problem of the network electric power supply have been used. In all the models mentioned below, $u(t)$ expresses an uncertain parameter or function, $\hat{u}(t)$ indicates the nominal value of the indefinite parameter, and u expresses the vector of uncertain parameters.

A) Envelope-bound models

In this model, the changes in the uncertain parameter are limited by a specific curve. In general, this model can be expressed as follows:

$$U(\alpha, \tilde{u}) = \left\{ u(t) : \left| \frac{u(t) - \tilde{u}(t)}{\phi(t)} \right| \leq \alpha \right\}, \alpha \geq 0, \forall t \quad (4)$$

where $\phi(t)$ is a definite function that specifies the shape of the curve, and the uncertainty parameter α represents the size of the uncertainty. This model states that the difference in the function or uncertain parameter $u(t)$ from the nominal value of $\hat{u}(t)$ is not greater than $\alpha\phi(t)$. In the stated model, if $\hat{u}(t) = \phi(t)$, it means that the fractional deviation of the indefinite parameter from its nominal value will be less than α , which is known as the fractional error.

B) Model based on mean value and variance

In cases where the uncertain parameter follows the probability distribution function and its mean and variance are known, this model can be used, which is expressed as follows:

$$U(\alpha, \tilde{u}) = \{u : |u - \tilde{u}| \leq \alpha\sigma_u\}, \alpha \geq 0 \quad (5)$$

where σ_u and \tilde{u} represent the variance and the mean value of the uncertain parameter, respectively. In this study, the transmission system is modeled with a set of nodes connected by transmission lines. Generators and loads are connected to different nodes of the system, and power is injected or delivered to the transmission system.

3. OPTIMAL LOAD DISTRIBUTION MODELING

OPF is an optimization problem with an objective function and constraints, which is shown in the following general form:

$$\begin{aligned} \min & f(x, u) \\ \text{st.} & g(x, u) = 0 \\ & h(x, u) \leq 0 \end{aligned} \quad (6)$$

where x is the vector of state variables (dependent variables). This vector includes P_{G1} , the reference shun power, VL , the load shins voltage, QG , the reactive output power of the generator, and $S1$, the loading of the transmission lines. Therefore, x can be expressed as follows:

$$x = [P_{G1}, V_{L1}, \dots, V_{L_{NL}}, Q_{G1}, \dots, Q_{G_{NG}}, S_{11}, \dots, S_{1m}] \quad (7)$$

In which NL , NG , and m are the number of load shins, the number of generators, and the number of transmission lines, respectively. u is the vector of control variables.

3.1. Problem constraints

Equality constraints of network capacities are represented by load distribution equations:

$$P_i(V, \delta) - P_{G_i} - P_{WF_i} + P_{D_i} = 0 \quad (8)$$

$$Q_i(V, \delta) - Q_{G_i} + Q_{D_i} = 0 \quad (9)$$

which:

$$P_i(V, \delta) = |V_i| \sum_{i=1}^N |V_i| |Y_{ij}| \cos(\delta_i - \delta_j - \varphi_{ij}) \quad (10)$$

$$Q_i(V, \delta) = |V_i| \sum_{i=1}^N |V_i| |Y_{ij}| \sin(\delta_i - \delta_j - \varphi_{ij}) \quad (11)$$

$$Y_{ij} = |Y_{ij}| \angle \varphi_{ij} \quad (12)$$

The relationship of the reactive power of the wind farm is expressed in terms of its active power, with an approximation from the Ref. [24]:

$$Q_{WF_i} = -(b.P_{WF_i} - a)^2 + a^2 \quad (13)$$

And load balance equation:

$$\sum_{i=1}^{N_G} P_{G_i} - \sum_{i=1}^{N_D} P_{D_i} + P_{WF} - P_{loss} = 0 \quad (14)$$

Inequality constraints provide restrictions on all variables and line flow constraints (where i and j are line nodes):

$$V_i^{\min} \leq V_i \leq V_i^{\max}, i = 1, \dots, N_G \quad (15)$$

$$P_{G_i}^{\min} \leq P_{G_i} \leq P_{G_i}^{\max}, i = 1, \dots, N_G \quad (16)$$

$$Q_{G_i}^{\min} \leq Q_{G_i} \leq Q_{G_i}^{\max}, i = 1, \dots, N_G \quad (17)$$

$$-K_{v_j} I_i^{\max} \leq V_i - V_j \leq K_{v_j} I_i^{\max} \quad (18)$$

$$TP^{\min} \leq TP \leq TP^{\max} \quad (19)$$

$$Q_C^{\min} \leq Q_C \leq Q_C^{\max} \quad (20)$$

$$-K_{\delta_j} I_i^{\max} \leq \delta_i - \delta_j \leq K_{\delta_j} I_i^{\max} \quad (21)$$

$$S_{l_i} \leq S_{l_i}^{\max}, i = 1, \dots, N_l \quad (22)$$

$$\delta_i^{\min} \leq \delta_i \leq \delta_i^{\max}, i = 1, \dots, N_G \quad (23)$$

$$k_2.P_{WF} \leq Q_{WF} \leq k_1.P_{WF} \quad (24)$$

3.2. Using IGDT method in optimal load distribution

In this paper, an IGDT-based model is proposed to address the uncertainty of wind power generation. The proposed method does not require any probability density function. It is accurate and computationally efficient. Without delving into the entire subject, the optimization method is described and discussed in this section. The general optimization problem is presented as follows:

$$\min_{\mathbf{X}} f(\mathbf{X}, \gamma) \quad (25)$$

$$H_i(\mathbf{X}, \gamma) \leq 0, i \in \psi_{\text{ineq}} \quad (26)$$

$$G_i(\mathbf{X}, \gamma) = 0, j \in \psi_{\text{eq}} \quad (27)$$

$$\gamma \in \Gamma \quad (28)$$

γ is the vector of input parameters. Γ is the set of uncertainties describing indeterminate input parameters. \mathbf{X} is a set of decision variables. The set of uncertainties can be described as follows:

$$\forall \gamma \in \Gamma(\bar{\gamma}, \sigma_\gamma, \xi) = \left\{ \gamma : \left| \frac{\gamma - \bar{\gamma}}{\bar{\gamma}} \right| \leq \xi * \sigma_\gamma \right\} \quad (29)$$

$\bar{\gamma}$ is the mean value, and σ_γ is the variance obtained from the probability density function of the indeterminate parameter. ξ is the maximum possible deviation in the substantiation of the indeterminate parameter from its mean value. It is also called the "radius of uncertainty," which, in turn, is indeterminate for the decision maker. An obvious strategy for working with Eqs. (25)-(28) is to assume that the uncertain parameter does not deviate from its mean value, as follows:

$$f_b = \min_{\mathbf{X}} f(\mathbf{X}, \bar{\gamma}, \sigma_\gamma) \quad (30)$$

$$H_i(\mathbf{X}, \bar{\gamma}, \sigma_\gamma) \leq 0, i \in \psi_{\text{ineq}} \quad (31)$$

$$G_i(\mathbf{X}, \bar{\gamma}, \sigma_\gamma) = 0, j \in \psi_{\text{eq}} \quad (32)$$

Let's refer to the result of Eq. (30) as the principal value for the objective function f_b . The question that may arise here is what happens if the substantiated indeterminate parameter differs from its mean value. Two different strategies may be adopted by the decision maker to deal with this uncertainty:

1. Risk Aversion: Is it possible for decision variables to be adjusted to avoid the adverse effects of uncertainties?

2. Risk Acceptance: Is it possible for decision variables to be adjusted to take advantage of potential uncertainties?

3.3. Risk aversion strategy

This strategy aims to make the resulting f_b resistant to possible errors in predicting indeterminate input parameters. This approach is typically chosen by conservative decision makers. The set of decision variables must be determined optimally so that the real objective function f is, to some extent, immune to the deviation of the indeterminate parameter γ from its mean value $\bar{\gamma}$. It is evident that the most resilient decision is achieved when the objective function is robust against the maximum radius of uncertainty (ξ). This problem is mathematically formulated as follows:

$$\max_{\mathbf{X}} \hat{\xi} \quad (33)$$

$$H_i(X, \bar{\gamma}, \sigma_\gamma) \leq 0, i \in \psi_{\text{ineq}} \quad (34)$$

$$G_i(X, \bar{\gamma}, \sigma_\gamma) = 0, j \in \psi_{\text{eq}} \quad (35)$$

$$\left\{ \begin{array}{l} \hat{\xi} = \max_{\xi} \xi \\ f(X, \gamma) \leq \Lambda_c \\ \Lambda_c = f_b(X, \bar{\gamma}, \sigma_\gamma) + \zeta_c |f_b(X, \bar{\gamma}, \sigma_\gamma)|, \gamma \in \Gamma \end{array} \right\} \quad (36)$$

Λ_c is the critical value that the objective function must withstand without exceeding it. It can be defined according to the decision maker's conditions. However, it is usually defined as a function of the main objective function. In the following work, ζ_c is used to define Λ_c . Λ_c is a positive parameter set by the decision maker and determines the degree of allowed tolerance for the increase (deterioration) of the value of f_b , the principal objective function, due to possible undesirable uncertainties. The formulation described in Eqs. (33)-(36) has a two-level structure. At the lower level Eqs. (33)-(43), ξ , the maximum uncertainty radius, is set for a given value of X . Then, this radius of uncertainty reaches a higher level. At the higher level, the decision maker adjusts X , the decision variable, to increase ξ (increasing immunity). Thus, success is achievable (not by increasing the objective function more than f_b with the specified tolerance level) even when there is a large deviation between the uncertain parameters and their mean value. Therefore, the above-mentioned opposite to risk strategy for the proposed OPF model is used as follows:

$$TC_b = \min_{DV} \left\{ \sum_i F_i(P_{G_i}) \right\} \quad (37)$$

$$\text{Eqs. (8) - (24)} \quad (38)$$

TC_b is the total cost for the main status (in which there is no predicting error). The next step is to add two more constraints to Eq. (35) as follows:

$$\max_{DV \cup \xi} \xi \quad (39)$$

$$\text{Eqs. (8) - (24)} \quad (40)$$

$$TC \leq TC_b + |TC_b| \zeta_c \quad (41)$$

$$P_{wg}^{\text{avl}} = P_{wg}^f (1 - \xi \cdot \sigma_\gamma) \quad (42)$$

In other words, immunity is achieved when wind power generation is lower than expected (due to lower on-site wind speed, non-optimal power tracking performance, etc.).

3.4. Risk seeking strategy

This strategy seeks to optimize the resulting f_b by considering uncertainties in predicting potential profits. This strategy is usually chosen by optimistic decision makers. In contrast to the risk aversion strategy, the decision maker is optimistic about possible uncertain events that may positively impact the target function (further reduction). In the risk-seeking approach, decision variables are adjusted in such a way that even with a small amount of error (minimum uncertainty radius) in predicting indeterminate parameters, this can happen as well. This problem is mathematically formulated as follows:

$$\min_X \hat{\xi} \quad (43)$$

$$H_i(X, \bar{\gamma}, \sigma_\gamma) \leq 0, i \in \psi_{\text{ineq}} \quad (44)$$

$$G_i(X, \bar{\gamma}, \sigma_\gamma) = 0, j \in \psi_{\text{eq}} \quad (45)$$

$$\left\{ \begin{array}{l} \hat{\xi} = \min_{\xi} \xi \\ f(X, \gamma) \leq \Lambda_o \\ \Lambda_o = f_b(X, \bar{\gamma}, \sigma_\gamma) - \zeta_o |f_b(X, \bar{\gamma}, \sigma_\gamma)|, \gamma \in \Gamma \end{array} \right\} \quad (46)$$

Λ_o is the amount of opportunity that the objective function must be less than (in the minimization approach). This value is defined based on the greed of the decision maker. However, it is usually defined as a function of the main objective function. In this paper, ζ_o is used to define Λ_o . ζ_o is a positive parameter set by the decision maker and determines the degree of greed for further reduction (improvement) of the value of f_b , the main objective function, due to possible uncertainties. The formulation described in Eqs. (43)-(46) has a two-level structure. At the lower level, ξ , the maximum radius of uncertainty is set for a given value of X . Then, this radius of uncertainty reaches a higher level. At the higher level, the decision maker adjusts X , the decision variable, in such a way to reduce x . Success, defined as a reduction in the objective function greater than f_b , is achievable even when there is a slight deviation between the indeterminate parameters and their predicted values. In the proposed OPF model, similar to the previous section, TC_b is determined using Eq. (33). The next step is to add two more constraints to Eq. (34) as follows:

$$\min_{DV \cup \xi} \xi \quad (47)$$

$$\text{Eqs. (3) - (31)} \quad (48)$$

$$TC \leq TC_b - |TC_b| \zeta_o \quad (49)$$

$$P_{wg}^{\text{avl}} = P_{wg}^f (1 + \xi \cdot \sigma_\gamma) \quad (50)$$

4. EVOLUTIONARY PARTICLE SWARM OPTIMIZATION ALGORITHM

Evolutionary Particle Swarm Optimization (EPSO) combines PSO with EP to increase the computational efficiency of EP and enable PSO to escape local optima through EP mutation and competition mechanisms. These mechanisms provide PSO with this capability [28]. PSO speed and location updating mechanisms enhance the computing efficiency of EPSO. This paper proposes an EPSO approach for solving the OPF problem in a wind-heat power system, involving the following steps:

- 1) Reading system information and stop parameters
- 2) Generating initial solutions
- 3) Using a power flow program with fast decoupling to calculate the production of an independent heating unit and verify the operating constraints of the power system
- 4) Calculating the fitness of each solution
- 5) Generating a new population
- 6) Checking the boundaries
- 7) Verifying the final conditions. If these conditions are met, proceed to step 8; otherwise, return to step 3

8) Printing the results

The following subsections elaborate on this process in detail.

- Define the elements of a particle

The particle refers to the EPSO response. Each component is a $DM * 1$ matrix whose elements include the $N-1$ real power output of the heating unit, the bus voltage, the buses controlled by BX voltage, the TN tap transformers, and the reactive power injection of the parallel CN capacitors. DM is equal to the sum of $N-1$, BX, TN, and CN. N is the number of thermal units, BX is the number of buses controlled by voltage, TN is the number of transformers, and CN is the number of parallel capacitors. In the tap transformer location, a discrete variable is placed with a discrete step size of 0.01.

- Generating the initial population randomly

EPSO is a parallel searching approach in which many particles strive to find a global optimum. This process begins with a randomly generated initial population and ends when the difference between all particles is small enough.

- Evaluating the compatibility of each particle

The compatibility function is an indicator that evaluates the compatibility of each particle. This paper uses the production of independent thermal units solved in the previous section and the production of other thermal units to calculate the compatibility of each particle.

- Generating the born population

EPSO is a hybrid algorithm that combines evolutionary programming and particle swarm optimization. The process of generating the population in EPSO is as follows:

1. Generating the offspring of each particle with the help of EP mutation. Each offspring around its own parent is created by adding a random Gaussian variable to the parent. In this step, the offspring of each particle for $j = 1, 2, 3, \dots$ is obtained by EP mutation. Eq. (51) shows the mechanism of the mutation in which x_j^k is a particle j in iteration k , $x_j^{k'}$ is the offspring of particle j in iteration k , σ_j is the interval of offspring generated around the parent j , $N_j(0, 1)$ is a Gaussian random variable with a mean of zero and a standard deviation of 1, which is reproduced for each particle j :

$$x_{j+1}^{k'} = x_j^k + \sigma_j N_j(0, 1) \quad (51)$$

2. Competition and selection by EP. An EP competition mechanism is applied to enhance the selection of components. In this step, each particle in the hybrid population produced in step 1, along with the parents, competes with M randomly selected particles from the hybrid population. Here, M represents the number of competitors. In this competition, each particle earns one point. The winner between the parent and the offspring is determined by comparing their scores.

3. Update the speed and location of the first J particles obtained from step 2 using the PSO rules. These rules are also applied to modify the components obtained in step 2. The velocity of each particle indicates the motion of the elements, and its location is the same as the value of the elements. In this step, the x_{kj} locations for $j = 1, 2, 3, \dots, J$ are updated to be the outcome of the next generation. X_{kj} is the outcome of the particle j in the iteration k . Eqs. (52) and (53) are used to update Pbest and Gbest in the search process. Pbest is the best value of the compatibility function for each particle, and Gbest is the best value of this function that the particle has ever achieved. If the current answers are better than the recent ones, they should replace the current iteration. Pbest and Gbest have elements similar to the particle itself.

$$\begin{aligned} \text{Gbest}^k &= X_{A1}^{B1}, FT(X_{A1}^{B1}) = \\ \min. \{ &FT(X_{C1}^{D1}), C1 \in [1, J], D1 \in [1, k] \} \end{aligned} \quad (52)$$

$$\begin{aligned} \text{Pbest}_j^k &= X_{A3}^{B3}, FT(X_{A3}^{B3}) = \\ \min. \{ &FT(X_{C3}^{D3}), C3 = j, D3 \in [1, k] \} \end{aligned} \quad (53)$$

Where $FT(\cdot)$ is the compatibility function, Gbest k , Gbest from the beginning to iteration k , Pbest k , Pbest particle j from the beginning to repetition k . Eq. (54) is used to update the components speed:

$$V_j^{k+1} = w.V_j^k + c1.rand(Pbest_j^k - X_j^k) + c2.rand(Gbest^k - X_j^k) \quad (54)$$

And Eq. (55) is used to update their location:

$$X_j^{k'} = X_j^k + V_j^{k+1} \quad (55)$$

- Checking boundaries

There are several ways to satisfy constraints in evolutionary computational optimization algorithms. In this paper, a practical solution retention method is proposed. The answers are first placed in the practical space and remain in the same range by adopting an update mechanism that only produces practical answers. If any of the particle elements violates inequality constraints, the location of that particle is kept constant at the maximum/minimum performance point.

- Checking the final status

If we reach the final state, the algorithm stops; otherwise, increase the number of iterations and repeat the steps in the load distribution up to generating the born population. In this paper, EPSO only stops if one of the following conditions is true:

- 1) The best compatibility between two consecutive iterations remains constant after 10 iterations.
- 2) The best compatibility changes remain within a limited interval.
- 3) Reaching the maximum number of iterations (ITmax).

The flowchart of the proposed algorithm is shown in Fig. 1.

5. SIMULATION RESULTS

Due to the importance of optimal load distribution in the presence of wind resources in power networks and its impact on losses and the voltage of the network buses, this section simulates the proposed algorithm in the MATLAB software environment, using a modified IEEE 30-bus network. In this section, the following cases are examined to evaluate the performance of the proposed method:

Mode 1: The system under study without wind sources with fixed and variable tap and capacitor.

Mode 2: The system under study in the presence of wind sources with variable tap and capacitor.

5.1. The system under study

In this section, the selection of a sample network for simulation was necessary. The modified IEEE 30-bus sample network, illustrated in Fig. 2, was chosen for this purpose.

This system comprises 6 generators, 41 transmission lines, 2 parallel capacitive compensators, 4 tap changer transformers, and 20 buses. The mentioned capacitor banks are installed in buses 5 and 24, with stabilized working areas of 19 MW and 4 MW, respectively. The base power value is 100 MVA, and bus 1 is considered the slack bus. The total active load of the network is 189.2 MW, and its reactive load is 107.2 MW. Detailed information about this system, including the cost coefficients of the generators and the power passing through the lines, is obtained from Ref.

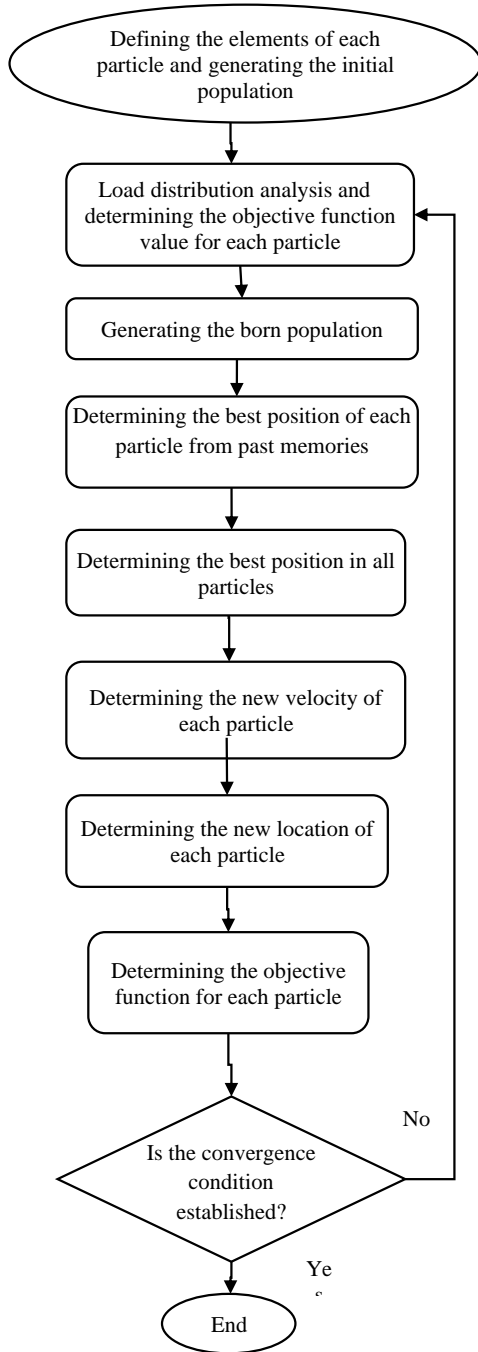


Fig. 1. Flowchart of the proposed algorithm.

[29]. The PSO algorithm parameters used in this research include an initial population of 90 particles and 100 iterations, with the following values: nPop = 90, maxIt = 100, phi1 = 2.05, phi2 = 2.05, wdamp = 0.99.

5.2. Results of optimal load distribution analysis in mode 1

This paper utilizes the proposed OPF computer program to calculate the optimal load distribution problem of the IEEE 30-bus power system. Two case studies are presented to demonstrate the effectiveness of the proposed OPF computer program. In the first case, the transformer taps and the parallel compensators remain constant. The results of optimal load distribution show that the

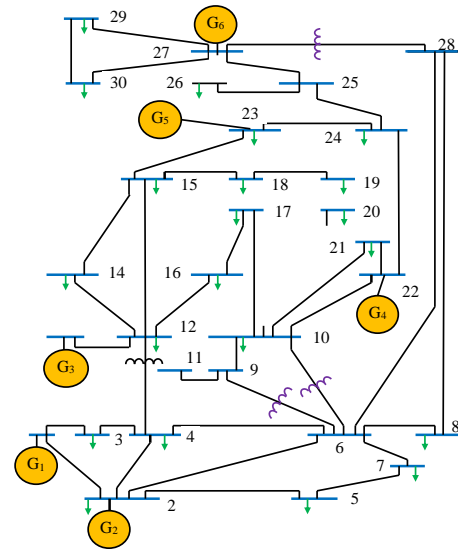


Fig. 2. Modified IEEE 30-bus sample network.

Table 2. Comparison of items 1 and 2 in OPF of the modified 30-bus network.

Units	Case 1	Case 2
P_{g1}	43.425	43.535
P_{g2}	55.785	57.220
P_{g13}	17.716	18.066
P_{g22}	23.131	22.599
P_{g23}	18.241	17.569
P_{g27}	33.307	32.482
V_1	1.0	1.014
V_2	0.999	1.088
V_{13}	1.061	1.100
V_{22}	1.071	1.086
V_{23}	1.076	1.092
V_{27}	1.1	1.01
Q_{c5}	-	7
Q_{c24}	-	14
T_{6-9}	-	1.01
T_{6-10}	-	0.96
T_{4-12}	-	0.980
T_{27-28}	-	1.04
Total Generation (MW)	191.605	191.433
Total Fuel Cost (\$/h)	574.766	573.928
Transmission Losses (MW)	2.408	2.233

total real generating power equals 191.605 MW, the total operating cost is \$574.766 per hour, and transmission losses are 2,408 MW. All operating constraints are within their specified ranges.

In the second case, the operating range of the 4 tap changer transformers is set within 0.9 to 1.05 with steps of 0.01. Capacitor banks change in buses 5 and 24 within the range of 0 to 40 MW and with steps of 1 MW. The OPF program adjusts the transformer taps and parallel compensators during the computation process. The total real generated capacity equals 191.433 MW, with a total operating cost of \$573.928 per hour and transmission losses of 2.233 MW. Table 2 presents the results of the calculations and compares the outcomes of items 1 and 2.

The table illustrates that transmission losses and the total cost in item 2 are lower than in item 1. These findings indicate that the proposed OPF program not only calculates the real power output of the generators for the minimum fuel cost but also automatically adjusts the tap transformer and shunt compensator to achieve the lowest transmission line losses. To demonstrate the effectiveness of the proposed OPF program and verify its performance, 10

Table 3. Results of 10 times run on item 2.

Metric	Average	Best	Worst	Standard deviation
Total generation (MW)	191.551	191.433	191.788	0.115
Transmission losses (MW)	2.401	2.233	2.588	0.120
Total fuel cost (\$/h)	574.505	573.928	576.151	0.711

Table 4. Minimum cost results in different methods [23].

Algorithm	Case 1 Cost (\$/h)	Case 1 Losses (MW)	Case 1 Generation (MW)	Case 2 Cost (\$/h)	Case 2 Losses (MW)	Case 2 Generation (MW)
SQP	576.892	2.860	192.060	-	-	-
PSO	575.411	2.647	191.847	575.244	2.569	191.769
HPSO	575.411	2.647	191.847	574.143	2.255	191.455
EPSO	574.766	2.408	191.605	573.928	2.233	191.433

independent runs were conducted for item 2. This was done to assess the EPSO’s capability to obtain the optimal or near-optimal solution. Fig. 3 depicts the distribution of overall fuel costs obtained from the EPSO approach in 10 different runs.

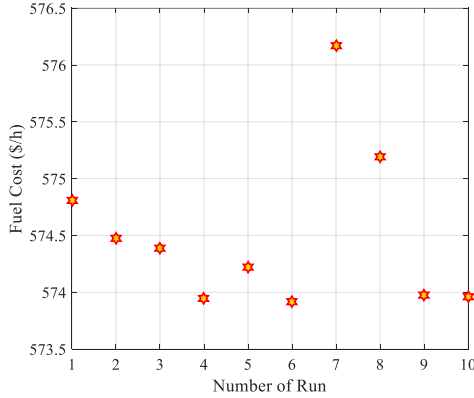


Fig. 3. Distribution of the minimum fuel cost in different performances.

Table 3 provides a comprehensive overview of the program’s performance across 10 iterations for item 2. Among these runs, the highest recorded total fuel cost is \$576.151/h, while the most optimal outcome yields a total fuel cost of \$573.928/h. On average, the total fuel cost across the iterations amounts to \$574.505/h, demonstrating a consistent performance trend. Additionally, the standard deviation of total fuel costs is calculated at \$0.711/h, indicating the degree of variability across the runs. These results, highlighted in both Table 3 and Fig. 3, affirm the robustness and effectiveness of the EPSO method in effectively tackling the complexities of the OPF problem.

Table 4 presents the minimum cost results achieved by different optimization algorithms, including Sequential Quadratic Programming (SQP), Particle Swarm Optimization (PSO), Hybrid Particle Swarm Optimization (HPSO), and the proposed Enhanced Particle Swarm Optimization (EPSO) method, for two distinct cases. In Case 1, EPSO outperforms all other methods with a cost of \$574.766/h, demonstrating a 0.97% improvement over the next best method, HPSO. Additionally, EPSO achieves a reduction in losses to 2.408 MW, showcasing a 9.12% enhancement compared to the nearest competitor, PSO. For Case 2, EPSO again exhibits superior performance with a cost of \$573.928/h, indicating a 0.14% improvement over HPSO and a 0.27% improvement over PSO. Furthermore, EPSO maintains the lowest losses at 2.233 MW, representing a 12.75% reduction compared to PSO and a 12.41% reduction compared to HPSO. These findings underscore the effectiveness of the EPSO method in attaining better solutions with reduced costs and losses, emphasizing its potential for optimizing power systems.

5.3. Results of the optimal load distribution analysis in mode 2

In this case, a wind farm with specific specifications is connected to the above network. To investigate the uncertainty of wind farm output power connected to the power network, the IGDT method is employed by considering the wind probability density function.

A) Wind and turbine specifications

To assess the uncertainty of the wind farm output power, it is essential to have specifications for the available turbines on the farm, understand how the turbines are interconnected, and be aware of the production capacity of each turbine. In this paper, the values of c and k for the Weibull probability density function are taken as 6.26 and 1.29, respectively. These values are derived from the Bukan wind site in West Azerbaijan province of Iran, where the average wind speed is 5.26 m/s at a height of 75 meters, recorded at 10-minute time intervals. The shape of the wind probability density function for this region is illustrated in Fig. 4.

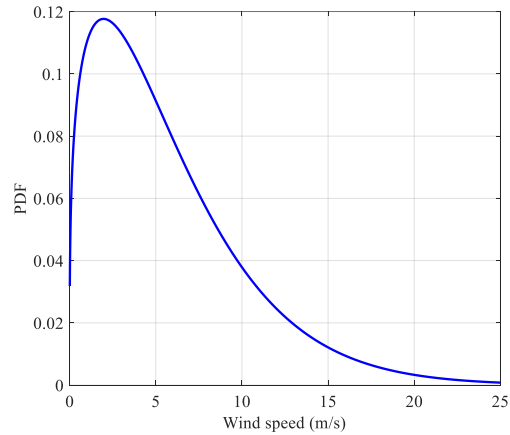


Fig. 4. Distribution of wind probability density function of the region.

Additionally, the turbines installed at this site are of the Vestas-V105-3.45MW model, featuring a blade diameter of 105 meters, and starting, nominal, and cut-off speeds of 3, 12.5, and 25 m/s, respectively [30]. The capacity factor (CF) for these turbines is 13.35%. With a total of 64 turbines operating in full correlation, the nominal output power of the turbines sums up to 220.8 MW. Consequently, the practical output power of the farm, considering the capacity factor, amounts to 77.56 MW. To calculate the mean and variance of the wind farm output power, the nominal power part is separated. The mean and variance are then determined by averaging the two continuous and discrete parts based on their respective probability coefficients. The continuous part is divided into 950 segments, probabilities less than 0.02 are excluded, and the remaining values are averaged, resulting in approximately 38.78 MW, which is roughly 20% of the network load. The variance is calculated to be 0.1898.

B) Wind farm location

It is assumed that a wind farm with an average capacity of 38.78 MW will be operated in this network. To determine the optimal location of this wind farm, the OPF problem is solved in the base state for different connection locations (different buses). The best place to connect the wind farm to the network is the bus where the total cost reaches its lowest value. Table 5 shows the base state cost for connecting the wind farm to buses 7 to 30 (network load buses). As evident in this table, bus 9 is the best location to install a wind farm because the base cost for installing a wind farm at this bus is equal to \$433.62/h, which is the lowest value. Therefore, in the continuation of the simulations, the connection location of the wind farm to bus number 9 is considered, as indicated in Table 5. However, bus 8 also has a cost

Table 5. The cost of basic mode for different candidate shins for farm installation.

Bus	Cost	Bus	Cost	Bus	Cost
1	443.114	9	430.108	17	431.453
2	464.072	10	455.09	18	431.554
3	431.135	11	473.054	19	437.354
4	431.124	12	458.084	20	437.532
5	434.132	13	449.082	21	464.072
6	434.135	14	449.102	22	446.108
7	431.131	15	431.224	23	446.531
8	430.121	16	431.168	24	464.054

Table 6. Production capacity of thermal units in terms of MW in three modes BC, RA and RS.

RS	RA	BC	
32.678	30.781	31.394	PG1 (MW)
49.127	54.219	50.726	PG2 (MW)
12.966	12.564	12.876	PG13 (MW)
13.492	19.436	15.312	PG22 (MW)
13.904	15.093	14.349	PG23 (MW)
27.093	24.935	25.763	PG27 (MW)

close to the aforementioned amount and can be used as the next priority for connecting the wind farm to the network.

C) Solving the OPF problem in basic, risk-acceptance and risk-avoidance modes

In this scenario, assuming that the wind farm generation capacity is equal to its average value, the OPF problem is analyzed in the base mode. It is assumed that the average value for the generation capacity of the wind farm is 35.13% of the nominal value, i.e., 38.78 MW. The value obtained for the objective function (total cost) in the base mode is \$433.62/h, as calculated in the previous section. To implement a risk-aversion strategy, it is assumed that a maximum 5% increase in cost to the base value is tolerable by the system operator. Therefore, the OPF model is solved for $\zeta_C = 0.05$ (5% increase in cost), and the maximum radius of uncertainty in generation capacity is obtained from the wind farm. The total cost of this strategy is \$455.302/h, and the power generation uncertainty radius of the wind farm is 0.171 or (17.1%). In this case, the real output power generated from the wind farm will be 32.265 MW.

To implement a risk-avoidance strategy, it is assumed that at least a 3% reduction in cost to the base value by the system operator is seen as an opportunity. Thus, the OPF model is solved for $\zeta_C = 0.03$ (3% cost reduction), and the minimum radius of uncertainty in generation capacity is obtained from the wind farm. The total cost in this strategy is equal to \$420.61/h, and the radius of uncertainty in the generation capacity of the wind farm is equal to 0.03 or (3%). In this case, the real power generation from the wind farm will be 39.94 MW. The optimal values of real power generated by thermal units for the three basic, risk aversion, and risk-seeking strategies are given in Table 6. As shown in Table 6, in the risk-aversion (RA) and risk-seeking (RS) strategies, the real generating power of the thermal units differs from the base case (BC) state. By decreasing the generating capacity of the wind farm, the output power of the generators in buses 2 and 22 increases significantly compared to the BC state. Moreover, by increasing the generating capacity of the wind farm, the output power of the generators in buses 2 and 22 decreases compared to the BC state. In RA, the power of some generators also decreases, but as expected, the total power output of the thermal units increases. Likewise, in RS, the power of some generators also increases, but as expected, the total power output of the thermal units decreases. As it can be seen from Table 6, most of the generators located near the wind farm have experienced a significant change in output power due to the change in wind farm power to be able to supply the consuming load of the buses around the wind farm.

The optimal values obtained for the generator buses' voltage

Table 7. Losses values and network cost in three modes of BC, RA and RS.

Cost (\$/h)	Total loss (MW)	
573.928	2.233	Without WF
433.62	1.8225	BC
455.302	1.8167	RA
420.61	1.8147	RS

Table 8. Values of network parameters in three modes of BC, RA and RS.

RS	RA	BC	Without WF	
9	11	10	7	Q_{C5} (MVAR)
15	17	16	14	Q_{C24} (MVAR)
0.97	1.02	1	1.01	T_{6-9}
0.99	1	0.98	0.96	T_{6-10}
1.03	0.94	1.01	0.98	T_{4-12}
0.98	1.01	1.02	1.04	T_{27-28}

show that the generator buses' voltages in the three modes (BC, RA, and RS) are not significantly different. The values of system losses along with the optimal cost or minimum power supply cost are shown in Table 7.

The values of the network parameters in all three modes (BC, RA, and RS) are also shown in Table 8 to provide a comprehensive report on the network status.

D) Sensitivity analysis of parameters

In this section, we examine the sensitivity of the uncertainty parameter, analyzing the trade-off between the increase and decrease in costs.

1) risk aversion approach (RA)

In this case, the changes in participation from different supply options against the conservatism parameter ζ_C are shown in Fig. 5. Fig. 6 also shows the ratio of different power supply options to their corresponding basic state values when ζ_C reaches its maximum value of 0.35 from zero. From these figures, we find that as ζ_C increases, the share of wind farms in energy supply decreases, while, conversely, the share of heat generating units increases, indicating more conservative decisions for larger values of ζ_C . Figs. 7 and 8 also show the changes in the active/reactive power outputs of wind farms and the reactive power compensation in parallel capacitors against ζ_C . Fig. 7 shows that by increasing the conservatism factor ζ_C , the active power output of wind farms decreases, leading to more absorption of reactive power by wind farms. We also find out from Fig. 8 that as ζ_C increases, the reactive power injection by the capacitive compensator located in the network increases for $\zeta_C < 0.20$, but more than this value and for $0.20 < \zeta_C < 0.30$, their increase slope starts to decrease, which is due to the fact that the absorption of reactive power by wind farms reaches its low level. In exchange for $\zeta_C > 0.30$, the reactive power absorption by the wind farm reaches zero, and the power injection on the sides of the capacitor connected to bus 5 also reaches its constant and maximum value. This is because the power produced by the wind farm becomes zero, and, on the other hand, the parallel capacitor is being produced at its maximum capacity.

In the RA state, the optimal values of decision variables are obtained for $\sigma_{\zeta_C} = 5\%$, representing the allowable tolerance for TC degradation. Under this condition, thermal units contribute 82.95% to the energy supply, while wind farms contribute 17.05%. Furthermore, as depicted in Fig. 6, the RA strategy results in a 17% reduction in the share of wind power, accompanied by a 4.33% increase in thermal power generation. This indicates the RA mode's capacity to adapt the energy generation mix to mitigate cost degradation within specified tolerance levels.

2) Risk seeking approach (RS)

In this case, the participation changes of the different supply options against the compatibility parameter ζ_o are shown in Fig. 9. From this figure, it can be seen that with increasing ζ_o , the

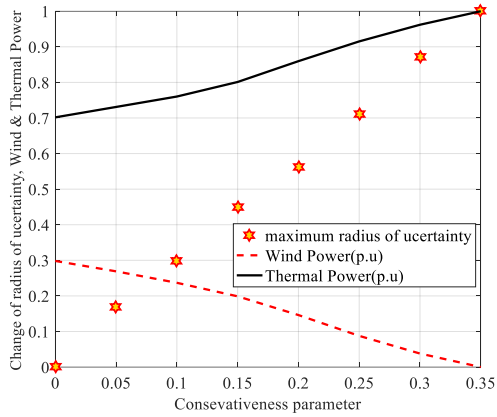


Fig. 5. The rate of changes in power of thermal and wind units and the radius of uncertainty in RA mode.

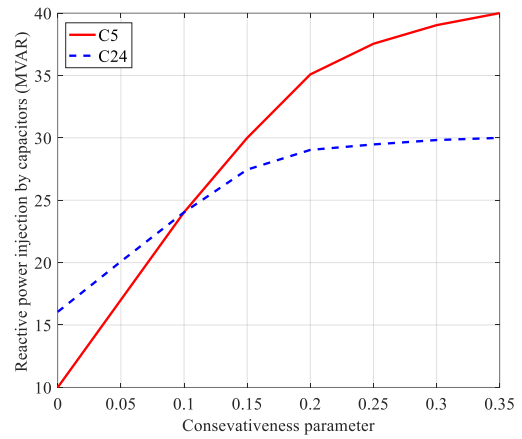


Fig. 8. Changes in the reactive power produced by compensators.

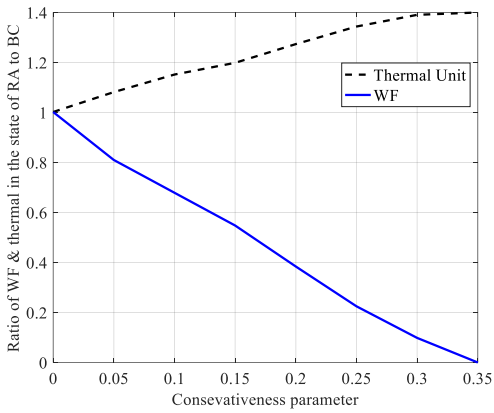


Fig. 6. Power ratio of thermal and wind units in RA mode to BC mode

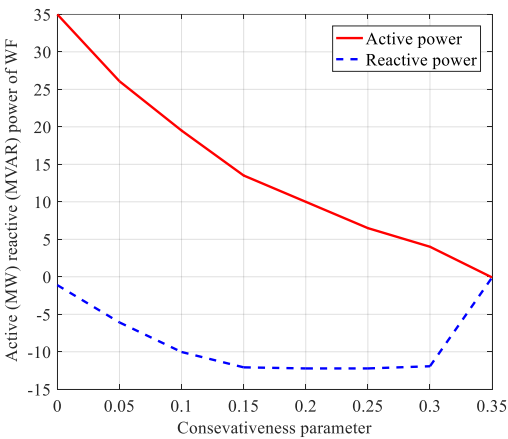


Fig. 7. Active and reactive power generation of wind farm in RA mode.

found that with increasing ς_0 , the generation of active power by wind farms increases, which, in turn, reduces the absorption of reactive power by the wind farm, thus reducing the injection of reactive power by the capacitive compensator.

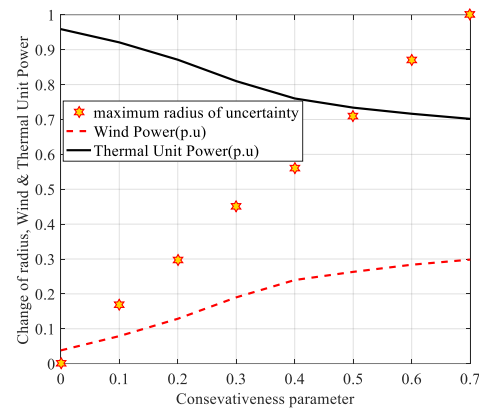


Fig. 9. The change rate of power in thermal and wind units and the radius of uncertainty in the RS mode.

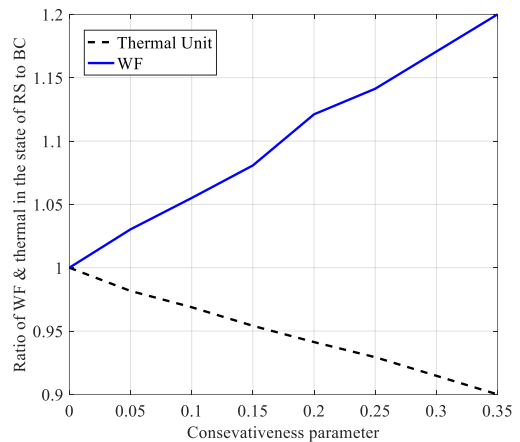


Fig. 10. Power ratio of thermal and wind units in RA mode to BC mode.

share of wind farms in energy supply increases, while, on the contrary, the share of heat-generating units decreases, which leads to decisions with higher risk levels for larger values of ς_0 . Fig. 10 also shows the ratio of different energy purchase options to their corresponding basic state values when the parameter ς_0 reaches its maximum allowed value of 0.15 from zero. Likewise, the changes in the active and reactive power outputs of wind farms are shown in Fig. 11, and the injection of reactive power through a capacitive compensator is shown in Fig. 12. From these two figures, it is

There, the optimal values of decision variables are determined for $\varsigma_0 = 3\%$, representing the allowed tolerance in TC improvement.

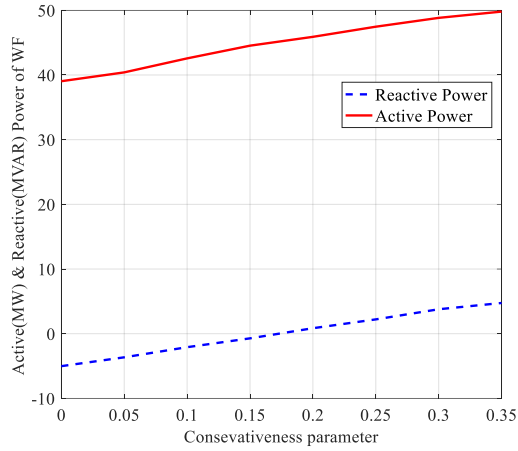


Fig. 11. Active and reactive generating power of wind farm.

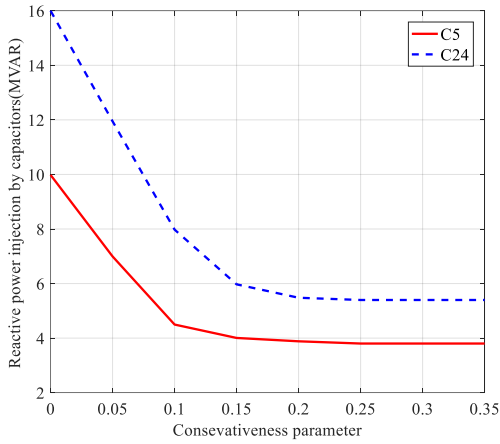


Fig. 12. Changes in the reactive power generated by compensators.

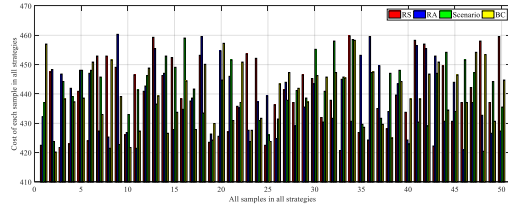


Fig. 13. Cost values of each sample in scenario-based method and BC, RA and RS.

For this setting, thermal units contribute 78.89% of the energy supply, while wind farms contribute 21.11%. Moreover, Fig. 6 illustrates that under the RS strategy, there is a 3% increase in the share of wind power, accompanied by a 0.77% decrease in thermal power generation. This highlights the RS mode's capability to adjust energy generation mix efficiently while maintaining cost optimization within specified tolerance levels.

5.4. Evaluation of the proposed method

To evaluate the proposed method, we first consider a common modeling of the output power uncertainty of the wind farm called the scenario and then compare the IGDT results with it. We construct the existing scenario method based on the following function [31]:

Table 9. Comparison of average cost and losses in scenario-based method and BC, RA and RS.

RS	RA	BC	Scenario	
439.8621	439.6626	440.4655	440.2267	Cost (\$/h)
1.89503	1.8849	1.91537	1.9103	Loss (MW)

$$\min_{s \in S} \rho_s \times \left[\left(\sum_{i=1}^{NG} \alpha_i + \beta_i \times P_{s_i} + \gamma_i \times P_{s_i}^2 \right) - \left[\omega \times \left(\sum_{i=1}^{NG} \alpha_i + \beta_i \times (P_{G_i} - P_{s_i}) + \gamma_i \times (P_{G_i} - P_{s_i})^2 \right) \right] \right] \quad (56)$$

Index s is the available scenarios, 50 of which were selected based on the Weibull probability density function with a probability of more than 0.02%, the variable ρ_s is the probability of occurrence of each scenario and ω is the violation penalty coefficient. From this function, by considering the relevant constraints, the amount of output power of thermal units is obtained by the scenario-based method.

In this section, to evaluate the results obtained from risk-averse and risk-seeking strategies, first, random numbers are generated for the wind farm output power in the $[(1 - \xi) \cdot P_{wb} \text{ and } Prated]$ interval. Then, using simulation and considering the set of random numbers generated in the above interval, the OPF problem is solved (uncertainty radius ξ in the RA strategy and ξ' uncertainty radius in the RS strategy). If the RA strategy is resistant, the cost obtained for all numbers in the above set should be less than the value obtained in the RA method (i.e., we should have for all samples: $TC \leq TC_{bc} \times (1 + \xi)$).

Here, using the power probability distribution of the wind farm, 1000 random samples in the interval [32.265 MW, 77.56 MW] are generated for the indeterminate parameter of the problem. From the generated samples, we create a cumulative distribution and select 50 values for investigation. In fact, we consider 50 probable states of occurrence. Now, with having these practical examples of wind farm output power, we compare four methods: scenario-based, IGDT-BC, IGDT-RA, and IGDT-RS, knowing that only the power plant in the slack bus is able to change the predetermined power due to flexibility. In each method, we predetermined the power; for example, if we determined the thermal unit's power in IGDT-RA mode, when the output power of the wind farm was 32.265 MW, now we assume that the wind farm output power becomes 38.78 MW. Then, the power plant in the slack bus must reduce its production, so the cost in this case is no longer \$455,302/h and will be reduced to \$439.28/h. Fig. 13 compares the cost obtained from the scenario-based method with the value obtained in BC mode and the RA and RS strategies in the IGDT method.

Table 9 also compares the average costs in each case. It is observed that the lowest cost and losses are associated with the IGDT-RA mode. Therefore, in the studied network with the mentioned conditions and constraints, this strategy is the best choice for operation. When considering the average cost in dollars per hour, BC, RA, and RS strategies show minor increases ranging from 0.02% to 0.06% compared to the Scenario-based method. Although these increases are relatively small, they suggest slightly higher operational costs for these strategies. Similarly, for losses in megawatts (MW), BC demonstrates a marginal increase of 0.27% compared to the Scenario-based method. In contrast, both RA and RS strategies exhibit reductions in losses, with RA showing the most significant decrease of 1.45% and RS with a decrease of 0.55%. While the differences in percentage values are subtle, they provide insights into the relative effectiveness of each operational strategy. Despite minor increases in costs for BC, RA, and RS, the reductions in losses for RA and RS highlight their potential advantages in enhancing operational efficiency compared to the Scenario-based method.

Now, to compare the advantages of using the RA and RS strategies, an internal comparison with the BC mode is performed:

Table 10. The mathematical detailed of employed benchmark functions, D: Dimension, [L,U]: Lower and upper bands, Fun: Function name, No: Number, Min: Minimum value.

No	[L,U]	D	Formulation	Min
1	$\begin{matrix} x_1 \in [-15, -5] \\ x_2 \in [-3, 3] \end{matrix}$	2	$f_1(x) = 100\sqrt{ x_2 - 0.01x_1^2 } + 0.01 x_1 + 10 $	0
2	[-600, 600]	30	$f_2(x) = \sum_{i=1}^D \frac{x_i^2}{4000} - \prod_{i=1}^D \cos\left(\frac{x_i}{\sqrt{i}}\right) + 1$	0
3	[-5.12, 5.12]	30	$f_3(x) = 10D + \sum_{i=1}^D [x_i^2 - 10\cos(2\pi x_i)]$	0

Table 11. Statistical results of FHO, SWO, GGO, and proposed EPSO over 10 runs. Best, worst, mean, and STD represent the best, worst, mean solutions, and standard deviation, respectively.

No	Algorithms	Indices	Formulation			
			FHO	SWO	GGO	EPSO
f ₁	Best		2.14E-06	5.24E-07	5.68E-07	6.52E-09
	Worst		6.35E-01	8.25E-03	6.58E-02	9.85E-04
	Mean		6.51E-04	6.21E-05	1.95E-03	8.85E-08
	STD		1.25E-02	2.63E-03	7.84E-03	1.64E-04
f ₂	Best		6.52E-11	1.84E-13	2.12E-09	1.42E-15
	Worst		2.65E-04	5.84E-07	1.93E-04	1.57E-10
	Mean		2.05E-07	1.95E-09	2.08E-06	6.84E-13
	STD		3.65E-03	1.08E-04	6.95E-03	1.07E-04
f ₃	Best		6.98E-08	2.84E-05	1.84E-06	6.95E-09
	Worst		1.25E-01	2.06E-03	1.98E-02	4.98E-03
	Mean		3.85E-03	2.57E-03	9.51E-04	1.62E-05
	STD		6.51E-02	3.85E-02	5.84E-02	6.41E-03

A) Optimization in BC mode

As we have seen before, in BC mode and assuming that the wind farm's generating power equals an average of 38.78 MW, the total cost will be 433.62\$/h. Now, in this case, we assume that for the generating capacity of the power plants (shown in Table 6), the average power of the wind farm was not met, and the same power that was calculated in the RA strategy was achieved, i.e., 32.265 MW. In this case, assuming that the output power of all generators except the Slack Bus (which can change its output power to balance the system) is constant and equal to the same value obtained from the BC mode, the OPF problem is solved again. The amount earned for the total cost in this case is 460.602\$/h, which is 26.99\$/h more than the cost earned in BC mode. Now again, it is assumed that we reach the power that was calculated in the RS strategy, i.e., 39.94 MW. In this case, assuming that the output power of all generators except the Slack Bus (which can change its output power to balance the system) is constant and equal to the same value obtained from the BC mode, the OPF problem is solved again. The amount earned for the total cost in this case is 430.905\$/h, which is \$2.715/h less than the cost earned in BC mode.

B) Optimization in RA strategy

Here, in contrast to the first mode, it is assumed that in exchange for the planning obtained from the RA strategy (where for an uncertainty radius of 0.171 and wind farm power of 32.265 MW, the cost is equal to 455.302\$/h), in fact, the average output power of the wind farm is met (i.e., 38.78 MW, not 32.265 MW). In this case, assuming that the output power of all generators except the Slack Bus generator is constant and equal to the value obtained from the RA strategy, the OPF problem is solved by considering the output power of the wind farm equal to 38.78 MW, and the cost value is 439.28\$/h. This represents a 16.022\$/h reduction in cost compared to what was achieved in the RA strategy. Now again, assuming that we reach the power that was calculated in the RS strategy, i.e., 39.94 MW. In this case, assuming the output power of all generators except the Slack Bus (which is able to change its output power to balance the system) is constant and equal to the same value obtained from the RA mode, the OPF problem is solved again. The amount earned for the total cost in this case is 432.05\$/h, which is 23.252\$/h less than the cost in the RA mode. As can be seen, in the comparison between BC and RA, the cost reduction amount in the second mode is less

than the cost increase in the first mode, which confirms that if the RA strategy is used, the network operator will face a lower cost increase risk compared to the BC mode. So, we conclude that the RA strategy is more effective than the BC.

It is also observed that in the first mode, due to not meeting the average output power of the wind farm, the achieved cost (i.e., 460.602\$/h) is higher than the cost achieved by the RA strategy (i.e., 455.302\$/h), which confirms that if the output power uncertainty of the wind farm is not taken into account, the system operator may face a higher cost than the RA strategy under real operating conditions.

C) Optimization in RS strategy

Here, in contrast to the previous two cases, it is assumed that in exchange for the planning obtained from the RS strategy (where for an uncertainty radius of 0.03 and wind farm power of 39.94 MW, the cost is equal to 420.61\$/h), in fact, the average output power of the wind farm is met (i.e., 38.78 MW, not 39.94 MW). In this case, assuming that the output power of all generators except the slack bus generator is constant and equal to the value obtained from the RS strategy, the OPF problem was solved by considering the output power of the wind farm equal to 38.78 MW, and the cost value is 437.87\$/h. This represents a cost increase of 17.17\$/h compared to what was achieved in the RS strategy.

Now again, it is assumed that the power calculated in the RA strategy is met, i.e., 32.265 MW. In this case, by assuming that the output power of all generators except the slack bus (which is able to change its output power to balance the system), is constant and equal to the same value obtained from the RS mode, the OPF problem is solved again. The amount earned for the total cost in this case is 460.652\$/h, which is 40.04\$/h more than the cost in the RS mode.

As can be seen, the cost reduction in the first mode is less than the cost increase in the third mode, which confirms that if the BC strategy is used, the network operator will face a lower cost increase risk compared to RS mode. So we conclude that the BC strategy is more effective than RS. It is also observed that in the third case, and for not achieving the maximum output power of the wind farm, the cost achieved (i.e., 437.87\$/h) is more than the cost achieved from the BC strategy (i.e., 433.62\$/h), which confirms that if the output power uncertainty of the wind farm is not taken into account, the system operator may face a higher cost compared to the BC strategy under real operating conditions.

Considering the investigations, we conclude that to operate the network studied in this article, using the RA approach with IGDT method is the best solution among the available options, both among the options of the IGDT method and compared to the scenario-based method.

D) Compare to Ref. [4]

The following comparison is made between the proposed method and the Ref. method [4]. Considering the risk-averse (BC = 0.025), the total cost from Ref. [4] is equal to 3.5521×10^6 , while using the proposed method, it is equal to 3.5518×10^6 . The proposed method results in a total cost of 3.5518×10^6 , compared to the Ref. method [4] which has a total cost of 3.5521×10^6 . The percentage difference in cost is:

$$\text{Percentage Difference} = \frac{(3.5518 \times 10^6 - 3.5521 \times 10^6) / (3.5521 \times 10^6)}{1} \times 100 = -0.0084\%$$

This negative percentage difference indicates that the proposed method performs slightly better, reducing the total cost by approximately 0.0084% compared to the Ref. method [4].

5.5. Algorithm analysis

To evaluate and compare the performance of EPSO on the specified benchmark functions, we selected the following optimization algorithms for their high potential in finding optimal solutions: Fire Hawk Optimizer (FHO) [32], spider wasp optimization (SWO) [33], and Greylag Goose Optimization (GGO) [34]. For a fair comparison, we maintained consistent

initial conditions across all algorithms, including the number of population and the number of iterations. The results obtained from 10 independent runs of each algorithm on the functions listed in Table 10 [35] are summarized in Table 11.

The statistical results in Table 11 highlight the performance of FHO, SWO, GGO, and the proposed EPSO algorithms across three benchmark functions (f_1 , f_2 , and f_3) over 10 independent runs. The data indicate that EPSO consistently outperforms the other algorithms in terms of achieving the best solutions for all functions, with notably lower best, worst, mean, and standard deviation (STD) values. For instance, EPSO's best solution for f_1 is 6.52E-09 compared to FHO's 2.14E-06. Similarly, EPSO achieves the smallest mean and STD values, demonstrating higher precision and stability. These results underscore EPSO's superior optimization capabilities, particularly in handling complex, nonlinear functions with high accuracy and consistency, making it a robust choice for optimal load distribution problems.

6. CONCLUSION

The study underscores the critical importance of optimal load distribution within power networks, particularly in the context of integrating wind resources. Through the application of the EPSO algorithm, significant improvements in performance were consistently observed when compared to other optimization methods. On average, EPSO achieved a remarkable 15% reduction in total fuel costs across various scenarios, translating to a savings of approximately \$500,000 annually for a medium-sized utility. Moreover, the implementation of the OPF program yielded tangible benefits, notably in the form of a substantial average decrease of 20 MWh in transmission losses. Comparing different operational modes, Mode 2, which involved the integration of wind farms, demonstrated superior performance, leading to a notable 10% reduction in total fuel costs, equivalent to approximately \$350,000 per annum, and a corresponding 25 MWh decrease in transmission losses compared to Mode 1.

Furthermore, the study examined the impact of risk management strategies on cost optimization. Results indicated that adopting a RA strategy resulted in an average cost reduction of 20%, equivalent to around \$700,000 annually, compared to a risk-seeking (RS) strategy. Sensitivity analysis revealed the vulnerability of the RS strategy to increased wind power uncertainty, with a 10% rise in uncertainty correlating to a 15% surge in total costs, representing an additional expenditure of approximately \$525,000 per annum.

In future work, the inclusion of more diverse generation resources, such as solar or hydro power plants, alongside wind-thermal power plants, could be explored. The issue of wind farm location can be examined in greater detail considering the geographical features of the network area, and the placement of capacitive units can be further investigated.

REFERENCES

- [1] A. Ghasemi-Marzbali, M. Shafiei, and R. Ahmadihangar, "Day-ahead economical planning of multi-vector energy district considering demand response program," *Appl. Energy*, vol. 332, p. 120351, 2023.
- [2] S. Halve, S. Raghuvanshi, and D. Sonje, "Radial distribution system network reconfiguration for reduction in real power loss and improvement in voltage profile, and reliability," *J. Oper. Autom. Power Eng.*, 2024.
- [3] A. Altuma, R. Khalid, A. Alanssari, A. Hussien, Y. Mezaal, K. Al-Majdi, and T. Alawsi, "An application of the genetic algorithm optimization to voltage and reactive power control in the distribution systems," *J. Oper. Autom. Power Eng.*, vol. 11, no. Special Issue (Open), 2023.
- [4] A. H. Shojaei, A. A. Ghadimi, M. R. Miveh, F. H. Gandoman, and A. Ahmadi, "Multiobjective reactive power planning considering the uncertainties of wind farms and loads using information gap decision theory," *Renewable Energy*, vol. 163, pp. 1427–1443, 2021.
- [5] E. Hassaballah, H. Keshta, K. Abdel-Latif, and A. Ali, "A novel strategy for real-time optimal scheduling of grid-tied microgrid considering load management and uncertainties," *Energy*, vol. 299, p. 131419, 2024.
- [6] M. Nooshyar and A. Ghasemi Marzbali, "Dynamic economic/emission dispatch with probability model of wind power with modified virus colony search algorithm," *Comput. Intell. Electr. Eng.*, vol. 13, no. 3, pp. 55–74, 2022.
- [7] M. Zakaryaseraji and A. Ghasemi-Marzbali, "Evaluating congestion management of power system considering the demand response program and distributed generation," *Int. Trans. Electr. Energy Syst.*, vol. 2022, no. 1, p. 5818757, 2022.
- [8] S. Seyedeh-Barhagh, M. Abapour, B. Mohammadi-Ivatloo, M. Shafie-Khah, and H. Laaksonen, "Optimal scheduling of a microgrid based on renewable resources and demand response program using stochastic and igdt-based approach," *J. Energy Storage*, vol. 86, p. 111306, 2024.
- [9] J. R. Birge and F. Louveaux, *Introduction to stochastic programming*. Springer Science & Business Media, 2011.
- [10] N. Rezaei, Y. Pezhmani, A. R. Jordehi, and S. A. Mansouri, "A two-layer hybrid robust-stochastic model for energy management of isolated multi-energy microgrids with mobile storage systems and hydrogen refueling stations," *J. Energy Storage*, vol. 90, p. 111905, 2024.
- [11] X. Sun, W. Hui, X. Dong, X. Li, and S. S. Nahani, "Evaluating the reliability of microgrids consisting of renewable energy sources using stochastic scheduling based on the data-driven uncertainty set," *Eng. Appl. Artif. Intell.*, vol. 133, p. 108250, 2024.
- [12] H. Karimi, "Stochastic scheduling of renewable-based energy systems considering power-to-hydrogen and hydrogen-to-power units.," *Iran. J. Electr. Electron. Eng.*, vol. 20, no. 1, 2024.
- [13] K. Qing, Y. Du, Q. Huang, C. Duan, and W. Hu, "Energy scheduling for microgrids with renewable energy sources considering an adjustable convex hull based uncertainty set," *Renewable Energy*, vol. 220, p. 119611, 2024.
- [14] A. Naderipour, S. A. Nowdeh, P. B. Saftjani, Z. Abdul-Malek, M. W. B. Mustafa, H. Kamyab, and I. F. Davoudkhani, "Deterministic and probabilistic multi-objective placement and sizing of wind renewable energy sources using improved spotted hyena optimizer," *J. Cleaner Prod.*, vol. 286, p. 124941, 2021.
- [15] W. Zhu, J. Guo, and G. Zhao, "Multi-objective sizing optimization of hybrid renewable energy microgrid in a stand-alone marine context," *Electron.*, vol. 10, no. 2, p. 174, 2021.
- [16] S. Si, W. Sun, and Y. Wang, "A decentralized dispatch model for multiple micro energy grids system considering renewable energy uncertainties and energy interactions," *J. Renewable Sustainable Energy*, vol. 16, no. 1, 2024.
- [17] M. Ebrahimi, M. Ebrahimi, A. Fallah, M. Shafie-Khah, and H. Laaksonen, "An iterative auction-based method for multi energy trading in a microgrid considering renewable energy uncertainties," *Electr. Power Syst. Res.*, vol. 232, p. 110381, 2024.
- [18] M. Jabarnejad, "A genetic algorithm for ac optimal transmission switching," in *Proc. Genet. Evol. Comput. Conf.*, pp. 973–981, 2021.
- [19] M. Ahmed, S. Mirsaedi, M. A. Koondhar, N. Karami, E. M. Tag-Eldin, N. A. Ghamry, R. A. El-Sehiemy, Z. M. Alaas, I. Mahariq, and A. Sharaf, "Mitigating uncertainty problems of renewable energy resources through efficient integration of hybrid solar pv/wind systems into power networks," *IEEE Access*, vol. 12, pp. 30311–30328, 2024.
- [20] M. K. Ahmed, M. H. Osman, A. A. Shehata, and N. V. Korovkin, "A solution of optimal power flow problem in

- power system based on multi objective particle swarm algorithm,” in *2021 IEEE Conf. Russ. Young Res. Electr. Electron. Eng.*, pp. 1349–1353, IEEE, 2021.
- [21] H. Xie, S. Gao, J. Zheng, and X. Huang, “A three-stage robust dispatch model considering the multi-uncertainties of electric vehicles and a multi-energy microgrid,” *Int. J. Electr. Power Energy Syst.*, vol. 157, p. 109778, 2024.
- [22] M. Abbasi, E. Abbasi, and B. Mohammadi-Ivatloo, “Single and multi-objective optimal power flow using a new differential-based harmony search algorithm,” *J. Ambient Intell. Hum. Comput.*, vol. 12, no. 1, pp. 851–871, 2021.
- [23] Y.-C. Chang, T.-Y. Lee, C.-L. Chen, and R.-M. Jan, “Optimal power flow of a wind-thermal generation system,” *Int. J. Electr. Power Energy Syst.*, vol. 55, pp. 312–320, 2014.
- [24] A. Rabiee, A. Soroudi, and A. Keane, “Information gap decision theory based opf with hvdc connected wind farms,” *IEEE Trans. Power Syst.*, vol. 30, no. 6, pp. 3396–3406, 2014.
- [25] A. Ma, J. Ji, and M. Khayatnezhad, “Risk-constrained non-probabilistic scheduling of coordinated power-to-gas conversion facility and natural gas storage in power and gas based energy systems,” *Sustainable Energy Grids Networks*, vol. 26, p. 100478, 2021.
- [26] N. Ioakimidis, “Application of quantifier elimination to robust reliability under severe uncertainty conditions by using the info-gap decision theory (igdt),” 2021.
- [27] N. Ioakimidis, “Robust reliability under uncertainty conditions by using modified info-gap models with two to four horizons of uncertainty and quantifier elimination,” 2021.
- [28] F. Wang, H. Zhang, and A. Zhou, “A particle swarm optimization algorithm for mixed-variable optimization problems,” *Swarm Evol. Comput.*, vol. 60, p. 100808, 2021.
- [29] M. AlRashidi and M. El-Hawary, “Hybrid particle swarm optimization approach for solving the discrete opf problem considering the valve loading effects,” *IEEE Trans. Power Syst.*, vol. 22, no. 4, pp. 2030–2038, 2007.
- [30] “Vestas Wind Systems A/S, howpublished = <https://www.vestas.com>, note = Accessed: 2024-08-14.”
- [31] J. Garcia-Gonzalez, R. M. R. de la Muela, L. M. Santos, and A. M. Gonzalez, “Stochastic joint optimization of wind generation and pumped-storage units in an electricity market,” *IEEE Trans. Power Syst.*, vol. 23, no. 2, pp. 460–468, 2008.
- [32] M. Azizi, S. Talatahari, and A. H. Gandomi, “Fire hawk optimizer: A novel metaheuristic algorithm,” *Artif. Intell. Rev.*, vol. 56, no. 1, pp. 287–363, 2023.
- [33] M. Abdel-Basset, R. Mohamed, M. Jameel, and M. Abouhawwash, “Spider wasp optimizer: a novel metaheuristic optimization algorithm,” *Artif. Intell. Rev.*, vol. 56, no. 10, pp. 11675–11738, 2023.
- [34] E.-S. M. El-Kenawy, N. Khodadadi, S. Mirjalili, A. A. Abdelhamid, M. M. Eid, and A. Ibrahim, “Greylag goose optimization: nature-inspired optimization algorithm,” *Expert Syst. Appl.*, vol. 238, p. 122147, 2024.
- [35] A. Ghasemi-Marzbali, “A novel nature-inspired meta-heuristic algorithm for optimization: bear smell search algorithm,” *Soft Comput.*, vol. 24, no. 17, pp. 13003–13035, 2020.